Applied Catalysis B: Environmental 209 (2017) 128–138

Contents lists available at ScienceDirect

Applied Catalysis B: Environmental

journal homepage: www.elsevier.com/locate/apcatb

Effect of Ni/Al molar ratio on the performance of substoichiometric $NiAl_2O_4$ spinel-based catalysts for partial oxidation of methane

Miryam Gil-Calvo, Cristina Jiménez-González, Beatriz de Rivas, Jose Ignacio Gutiérrez-Ortiz, Rubén López-Fonseca *

Chemical Technologies for Environmental Sustainability Group, Department of Chemical Engineering, Faculty of Science and Technology, University of The Basque Country UPV/EHU, P.O. Box 644, E-48080 Bilbao, Spain

ARTICLE INFO

Article history:
Received 29 November 2016
Received in revised form 1 February 2017
Accepted 18 February 2017
Available online 21 February 2017

Keywords:
Methane
Partial oxidation
Nickel aluminate
Substoichiometric spinels

ABSTRACT

The viability of a series of nickel aluminate-based spinel catalysts with varying Ni deficiency (corresponding to a Ni/Al molar ratio in the 0.13–0.50 range) was explored for the partial oxidation of methane under different operation conditions in terms of temperature, volume hourly space velocity, O/C molar ratio and time on stream. Thus spinel-type catalysts with a Ni loading between 11 and 31 wt.% were prepared by coprecipitation. A wide number of techniques including WDXRF, XRD, N_2 physisorption, Raman spectroscopy, XPS, UV–vis-NIR DRS, H_2-TPR, TEM and TGA-MS were used to characterise the calcined, reduced and post-run samples.

With respect to the reference stoichiometric sample (Ni/Al = 0.50) alumina excess in the precursor oxide provoked notable changes in the surface area, structural properties connected with the relative cation distribution between tetrahedral and octahedral coordination and reducibility of the resultant spinel phase. It was found that the catalytic performance of these non-stoichiometric samples could be optimised for a Ni/Al molar ratio of 0.25, which corresponded to a metal loading of 19 wt.%Ni. The oxidation activity was associated with the remarkable intrinsic activity of nickel particles derived from Ni^{2+} cations with a preferential occupancy of octahedral sites in the lattice of the oxide. The promising catalytic behaviour of this sample was further proven by the notable activity and stability shown under severe reaction conditions with a reduced loss of yield of hydrogen with time on stream.

1. Introduction

Along with the important role played by hydrogen in the chemical industry and more particularly in the refining of oil and the synthesis of chemical products, more recently hydrogen has received increased interest as potential energy source for fuel cells owing to its high energy conversion efficiency. Typically hydrogen is produced by fossil fuel reforming, particularly by reforming of natural gas (methane), because of its abundance, easy availability and high yield of hydrogen per carbon atom in the feed. In this sense, catalytic partial oxidation is often considered as an emerging oxidation alternative to steam reforming, which is currently the state-of-the-art process for commercial hydrogen and syngas production, since it advantageously requires less energy input and no water is needed.

Nickel catalysts are widely recognised as suitable candidates for avoiding the use of noble metals in catalyst formulation for a wide range of methane-to-syngas processes including partial oxidation. The interest is justified on the basis of the fact that nickel-based catalysts usually offer a good balance between performance and limited cost. As a consequence much attention has been given to designing new improved catalytic systems with a relatively low cost. The main requirement of active nickel samples is associated with a high metallic dispersion, which in turn controls activity, stability and resistance towards coking and sintering. To achieve this goal an appropriate strategy for catalyst synthesis is to introduce the transition metal into the structure of a crystalline precursor oxide such as hexaaluminates [1,2], hydrotalcites [3,4], perovskites [5,6] or spinels [7,8] instead of the conventional route consisting of anchoring NiO onto a high surface support.

Spinel-type oxides with a chemical formula of AB_2O_4 are particularly interesting since these posses a wide range of cation distribution. Typically the divalent and trivalent cations fill tetrahedral and octahedral sites, respectively, which is known as the normal distribution. However, nickel aluminate is a class of spinel oxide with the so-called inverse distribution where the trivalent cations preferentially occupy the tetrahedral sites while the octahedral sites are filled by both divalent and trivalent cations [9].

* Corresponding author.
E-mail address: ruben.lopez@ehu.eus (R. López-Fonseca).

http://dx.doi.org/10.1016/j.apcatb.2017.02.063
0926-3373/

In this sense the use of Ni/Al_2O_3 catalysts derived from $NiAl_2O_4$ has shown promising results for reforming applications [10–14] due to their thermal stability, high surface area and relatively disperse metallic nickel on stable alumina, which are obtained after a suitable activation by high-temperature reduction of nickel ions present in the crystalline lattice. Thus strong interactions can be expected between the metallic species and the parent oxide support as a result of the confinement effect provided by the spinelic phase.

Perhaps one of the main disadvantages of stoichiometric $NiAl_2O_4$ is the remarkably high Ni loading (33 wt.% theoretically) and the higher cost of Ni with respect to Al, which is about 6 times higher. Therefore it would be of interest to develop spinel-based catalytic precursors that could provide the same or better catalytic properties than the reference stoichiometric phase in terms of surface area, Ni particle size, available metallic surface area and specific activity of Ni particles. The potential of non-stochiometric nickel aluminate-derived catalysts for methane-to-syngas processes has been scarcely studied in the literature. In this sense noteworthy are the works by Ubaid and Wolf [15] and Salhi et al. [16] related to the steam reforming and dry reforming of methane, respectively, and more recently the work by Zhang et al. [17] on the dry reforming of methane. All these studies pointed out the viability of controlling the composition of the spinel for achieving optimised nickel catalysts. However, increased efforts are necessary to understand the physico-chemical changes derived from non-stoichiometric formulations with respect to the base spinel (Ni/Al = 0.50) which eventually may have an important influence on the catalytic behaviour, particularly on the partial oxidation of methane.

The present study has therefore a two-fold objective: one is to thoroughly characterise a wide range of substoichiometric nickel aluminate spinels with a Ni/Al ratio in the 0.13–0.50 range in both calcined and reduced states; the other is to analyse the suitability of these materials reduced at high temperatures as potential catalysts for the partial oxidation of methane under different reaction conditions.

2. Experimental

2.1. Preparation of the spinel-based precursors

The spinel catalytic precursors were prepared by the coprecipitation method using varying amounts of aqueous solutions of $Ni(CH_3\text{-}COO)_2{\cdot}4H_2O$ and $Al(NO_3)_3{\cdot}9H_2O$ in the presence of ammonium hydroxide to adjust the final pH at 8. The use of nickel acetate instead of nickel nitrate can give additional advantages in terms of dispersion and crystallite size of the resultant catalyst [18]. The samples were denoted as Ni/Al(x) where x stands for the Ni/Al molar ratio of the sample, which was between 0.50 (for the stoichiometric sample) and 0.13. In this way a set of seven samples was obtained with a nickel content from 31 to 11 wt.%, respectively. For comparative purposes γ-Al_2O_3 was also prepared by precipitation following the same synthesis route. All samples were dried at 110 °C overnight and then calcined at 850 °C in static air for 4 h at a heating rate of 10 °C min^{-1}. Finally, pellets were prepared by a process of compressing the powders into flakes in a hydraulic press (Specac), crushing and sieving (0.3–0.5 mm).

2.2. Characterisation of the calcined and reduced samples

The calcined oxides were characterised by wavelength dispersive X-ray fluorescence (WDXRF), N_2 physisorption at −196 °C, X-ray diffraction (XRD), Raman spectroscopy, X-ray photoelectron spectroscopy (XPS), ultraviolet-visible-near infrared diffuse reflectance spectroscopy (UV–vis-NIR DRS) and temperature-programmed reduction with hydrogen (H_2-TPR) while the freshly reduced catalysts were analysed by N_2 physisorption, XRD and transmission electron microscopy (TEM). On the other hand, the post-run samples were studied by BET measurements, XRD, Raman spectroscopy, TEM and dynamic thermogravimetry coupled to mass spectrometry (TGA-MS). The experimental details of each analytical technique are described elsewhere [19–21].

2.3. Catalytic activity

Catalytic tests were performed in a bench-scale fixed-bed reactor (Microactivity modular laboratory system provided by PID Eng&Tech S.L.) operated at atmospheric pressure and fully monitored by computer. The reactor was made of stainless steel with an internal diameter of 9 mm and a height of 305 mm, in which the temperature was controlled with a thermocouple placed in the catalyst bed. Typically 0.125 g of catalyst in powdered form was loaded. The particle size was between 0.3–0.5 mm. In order to avoid hot spot formation or temperature gradients, the catalyst bed was diluted with inert quartz (1–1.25 mm, 0.875 g). The partial oxidation of methane reaction was studied with a feed gas mixture of 10%CH_4 and 5%O_2 balanced with N_2, with a total flow rate of 800 mL min^{-1} (38400 mL CH_4 g^{-1} h^{-1}) at two different temperatures, namely 650 and 700 °C, over a reaction time interval of 3 h. Additionally, the optimal catalyst was evaluated at 650 °C under more severe reaction conditions with a higher volume hourly space velocity (VHSV) (60000 mL CH_4 g^{-1} h^{-1}), a substoichiometric oxygen supply (O/C = 0.8) and a longer reaction time interval (30 h). Prior to the reaction, the synthesised catalytic precursors were activated in situ by reduction with 5%H_2/N_2 at 850 °C for 2 h. Feed and effluent streams were analysed online by a MicroGC (Agilent 3000) equipped with a TCD detector. Two columns, Molecular Sieve 5A and Plot U, were used in a series/bypass arrangement for the complete separation of H_2, N_2, O_2, CH_4, CO and CO_2. A cold trap at the outlet of the reactor was used to condense out any water from the product gas stream. On the basis of the molar flow at the inlet and outlet of the reactor, conversion and product yields were calculated, according to the following equations:

$$X_{CH_4}\% = \frac{F_{CO_{out}} + F_{CO_{2,out}}}{F_{CH_{4,in}}} \cdot 100 \quad (1)$$

$$Y_{H_2} = \frac{F_{H_{2,out}}}{2 \cdot F_{CH_{4,in}}} \quad (2)$$

$$Y_{CO} = \frac{F_{CO_{out}}}{F_{CH_{4,in}}} \quad (3)$$

$$Y_{CO_2} = \frac{F_{CO_{2,out}}}{F_{CH_{4,in}}} \quad (4)$$

The thermodynamic data were calculated via the HSC Chemistry software package by the GIBBS programme using the so-called Gibbs Energy Minimisation Method. In addition to solid carbon, the following gaseous substances were considered: CH_4, O_2, N_2, CO, CO_2, H_2 and H_2O.

3. Results and discussion

3.1. Catalytic behaviour of the Ni/Al(x) spinel-based catalysts in the partial oxidation of methane

In a previous paper we confirmed that the so-called indirect or combustion-reforming mechanism could explain the partial oxidation process over various Ni/Al_2O_3 catalysts prepared from nickel

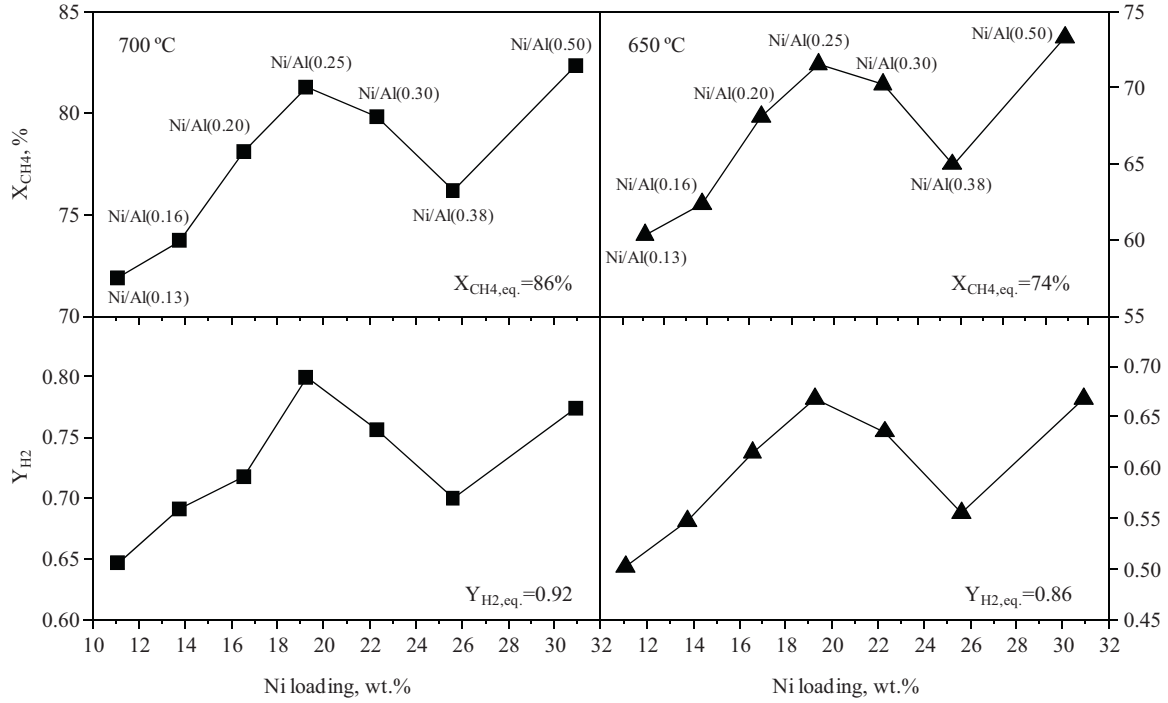

Fig. 1. Catalytic performance of the Ni/Al(x) catalysts in the partial oxidation of methane (reaction conditions: O/C = 1; 38400 mL CH_4 g^{-1} h^{-1}; 3 h, 650 and 700 °C).

Table 1
Methane conversion, yield to H_2, CO and CO_2 and H_2/CO and CO/CO_2 molar ratios over the Ni/Al(x) catalysts in the partial oxidation of methane (reaction conditions: O/C = 1; 38400 mL CH_4 g^{-1} h^{-1}; 3 h, 650 and 700 °C).

Catalyst	700 °C						650 °C					
	X_{CH4}, %	Y_{H2}	Y_{CO}	Y_{CO2}	H_2/CO	CO/CO_2	X_{CH4}, %	Y_{H2}	Y_{CO}	Y_{CO2}	H_2/CO	CO/CO_2
NiAl(0.50)	82	0.77	0.69	0.13	2.2	5.3	73	0.67	0.55	0.18	2.4	3.0
NiAl(0.38)	76	0.70	0.64	0.12	2.2	5.3	65	0.56	0.47	0.18	2.4	2.6
NiAl(0.30)	80	0.76	0.69	0.11	2.2	6.5	70	0.64	0.54	0.16	2.3	3.4
NiAl(0.25)	81	0.80	0.68	0.13	2.3	5.1	72	0.67	0.52	0.19	2.6	2.7
NiAl(0.20)	78	0.72	0.67	0.11	2.1	6.0	68	0.61	0.52	0.16	2.4	3.2
NiAl(0.16)	74	0.69	0.55	0.18	2.5	3.0	62	0.55	0.38	0.25	2.9	1.5
NiAl(0.13)	72	0.65	0.59	0.13	2.2	4.7	60	0.50	0.42	0.18	2.4	2.3

aluminate [22]. The first step of the reaction scheme was the complete combustion into CO_2 and H_2O with a concomitant exothermal event followed by reforming of the remaining unreacted methane with CO_2 and H_2O to give CO and H_2. Consequently the selection of the reaction temperature for comparing the performance of the catalysts in the partial oxidation reaction is important since a high combustion activity and a low yield of hydrogen are often observed at low temperatures (<600 °C). On the contrary, an eventual analysis carried out at relatively high temperatures (>750 °C) may result in a similar catalytic oxidation activity due to the fast kinetics of the process. For these reasons the behaviour of the Ni/Al(x) catalysts was firstly evaluated at 700 °C. These preliminary reaction tests were carried out at a VHSV of 38400 mL CH_4 g^{-1} h^{-1} with an O/C molar ratio of 1 over a relatively short reaction time interval (3 h). Conversion data were taken at 20 min-intervals. It must be pointed out that a notable increase in inlet temperature of about 25 °C was observed when the feed was first admitted to the reactor as a result of the occurrence of the combustion reaction (Fig. S1). With time on stream the inlet temperature gradually tended to achieve the given reaction temperature (700 °C). For this reason the first analysis of the feed exiting the reactor was performed after a 20 min interval so as to ensure that the composition of the corresponding product stream was not affected by these hot spots. Fig. 1 depicts the evolution of methane conversion and yield of hydrogen as a function of the composition of the spinel. It must be stated that these values were stable for all samples. Therefore the reported data corresponded to the average values over this time span. The catalysts with a Ni content higher than 14 wt.% achieved a notable activity with conversion values around 77–82%, which was relatively close to that predicted by the thermodynamic equilibrium ($X_{CH4,eq.}$ = 86%). Only the spinels with the lowest Ni content, namely Ni/Al(0.13) and Ni/Al(0.16), showed a somewhat lower conversion (72 and 74%, respectively). In view of these results two observations were noteworthy. Firstly, up to four substoichiometric samples (17–26 wt.%Ni) almost exhibited an oxidation activity as high as that noticed for the Ni/Al(0.50) catalyst. Secondly, a comparable conversion was attained over these four Ni-deficient samples. Analogously Enger et al. [23] did not find substantial differences in the activity of a series of $NiAl_2O_4$-based catalysts with a Ni content in the 14–26 wt.% range for the partial oxidation at 800 °C. Looking at the yield of hydrogen, although both Ni/Al(0.50) and Ni/Al(0.25) catalysts gave a virtually identical conversion (82 and 81%, respectively), the substoichiometric sample slightly yielded more hydrogen (Y_{H2} = 0.80 compared with Y_{H2} = 0.77 as shown in Table 1). This was assigned to a favoured conversion of CO into CO_2 and H_2 over the Ni/Al(0.25) catalyst as revealed by its somewhat higher H_2/CO molar ratio (2.3 compared with 2.2) and lower CO/CO_2 molar ratio (5.1 compared with 5.3). In sum, in view of

the results obtained over the samples with x < 0.50 an optimised behaviour was seen for the Ni/Al(0.25) catalyst since significantly lower yields were found for samples with lower and higher Ni content than 19 wt.%. The active sites for the partial oxidation process were metallic nickel. These sites were obtained after submitting the various spinel precursors to a high-temperature reduction step. On the other hand, it must be indicated that no methane conversion was observed over bare alumina, thereby suggesting that gas-phase reactions were irrelevant at this reaction temperature [22].

With the aim of determining that this oxidation pattern was also valid for lower reaction temperatures, thereby minimising the possible influence of fast kinetics on the achieved results at 700 °C, a new set of reaction runs at 650 °C was conducted while keeping constant the previously examined operation conditions. The corresponding catalytic results (conversion and yield of hydrogen) are also included in Fig. 1. Again these data corresponded to the average values measured each 20 min. The samples exhibited a high stability with time on line. Thus, the activity trend of the Ni/Al(x) samples was as follows: Ni/Al(0.50) ≈ Ni/Al(0.25) ≈ Ni/Al(0.30) > Ni/Al(0.20) ≈ Ni/Al(0.38) > Ni/Al(0.16) ≈ Ni/Al(0.13). The attained conversion over these three groups of catalysts was 70–73%, which was virtually identical to that predicted by thermodynamics ($X_{CH4,eq.}$ = 74%), 65–68% and 60–62%, respectively. Although these variations in conversion were appreciable, much more marked differences were noticed in the yield of hydrogen. Note that, on one hand, this is a more relevant reaction parameter from a practical point of view and besides, the measured values in the 0.50–0.67 range are not influenced by thermodynamics limitations since the equilibrium yield was 0.86. Accordingly the same pattern was noted when the yield of hydrogen was considered. Both Ni/Al(0.25) and Ni/Al(0.50) samples thus showed the best performance (Y_{H2} = 0.67). Therefore, on the basis of the performance of the synthesised spinels at 650 °C, the optimised behaviour of the Ni/Al(0.25) catalyst with a 19 wt.%Ni was proven. These results were in good agreement with those reported by Zhang et al. [17] who found that the composition of a series of mesoporous $NiAl_2O_4$/γ-Al_2O_3 composites could be suitably tuned for the dry reforming of methane. Thus the highest conversion was obtained for a composite with a 16–19 wt.%Ni loading. Similarly Kim et al. [24] pointed out that mesoporous alumina catalysts that incorporated nickel with a metal loading of 14–20 wt.% resulted highly active in the partial oxidation of methane. On the other hand, H_2/CO ratios were around 2.3–2.9 (Table 1). This suggested that the samples were significantly active in the reverse water gas shift reaction. The activation of this reaction by temperature leading to significant amounts of CO was evident since the H_2/CO ratio was 2.1–2.5 at 700 °C. Simultaneously the CO/CO_2 molar ratio increased from 1.5–3.4 at 650 °C to 3.0–6.5 at 700 °C (Table 1).

3.2. Characterisation of the spinel-based precursors

In order to rationalise the observed behaviour of the prepared spinel-based catalysts the structural, textural and surface properties of the calcined and reduced samples were extensively characterised.

To begin with, the structural properties of the calcined spinel-based catalytic precursors were investigated by X-ray diffraction. The corresponding patterns are depicted in Fig. 2. For comparative purposes the pattern of the as-synthesised γ-Al_2O_3 was also added. The main diffraction peaks of the Ni/Al(0.50) stoichiometric spinel were in good agreement with the JCPDS 78-1601 data of the face-centred cubic structure of nickel aluminate (space group *Fd*-3m). Thus, the signals at 2θ values of 19.1°, 31.4°, 37.0°, 45.0°, 59.6°, 65.5°, 78.8° and 83.1° were assigned to the (111), (220), (311), (400), (511), (440), (622) and (444) diffraction planes of the $NiAl_2O_4$ spinel, respectively. In order to calculate the unit cell parameters

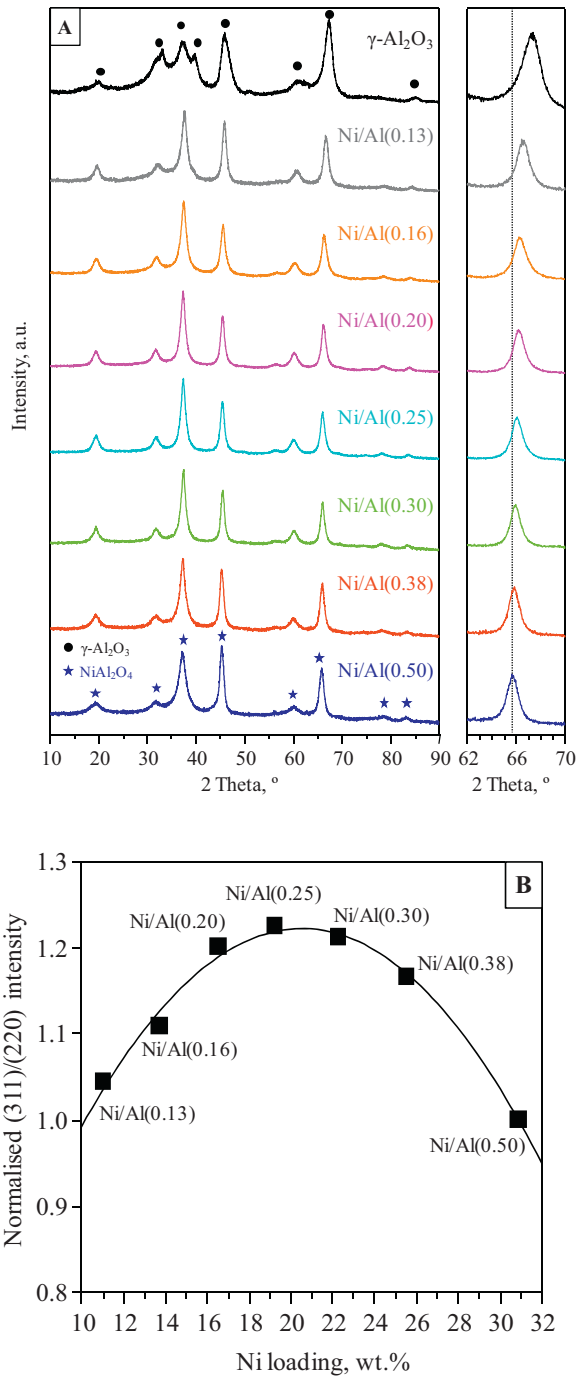

Fig. 2. XRD patterns of the Ni/Al(x) spinel-based precursors (A). Evolution of the normalised (311)/(220) intensity ratio as a function of the composition of the spinel (B).

the XRD patterns were processed using the full-profile refinement without structural model by FullProf software. The lattice constant was 8.050 Å, which was comparable to the value reported in the literature for a stoichiometric $NiAl_2O_4$ calcined between 850 and 900 °C [16,25]. For all substoichiometric samples the diffraction analysis indicated only the formation of the spinel structure. Furthermore, the absence of diffraction lines not assigned to a spinel-type phase, such as NiO with signals at 2θ values of 43.3° and 62.9° (JCPDS 78-0643), provided a strong evidence for a solid solution formation between alumina excess and nickel spinel irrespective of the Ni/Al molar ratio. This finding was consistent with the results from Yoo et al. [26] who also observed a continuous solid

solution for alumina excess magnesium aluminate spinels with a Mg/Al ratio between 0.05 and 0.50.

On the other hand, as the amount of alumina in the solid solution increased, the 2θ for the spinel peaks monotonically shifted to a higher value [27]. As a consequence, the lattice constant almost linearly decreased from 8.050 Å for the Ni/Al(0.50) sample to 7.956 Å for the Ni/Al(0.13) sample, and approached the lattice constant value (7.891 Å) of the as-synthesised pure γ-alumina (Fig. S2, Table 2). This decrease in the unit cell parameter for a substoichiometric spinel (Ni/Al = 0.13) was also found by Otero-Arean et al. [25]. This contraction was expectedly observed because Al^{3+} (54 pm) is smaller than Ni^{2+} (69 pm) in terms of ionic radius. Furthermore, this shrinkage of the lattice could be promoted owing to the formation of oxygen vacancies induced by charge compensation mechanisms [28].

Apart from the shift in diffraction angles, a notable difference in the relative intensity ratios of the peaks was also found for the various substoichiometric samples with respect to the Ni/Al(0.50) spinel. This may suggest substantial changes in the distribution of cations with the composition of the Ni/Al(x) spinel. In this sense it is widely accepted that the diffraction lines associated with the (220) plane are related to the tetrahedrally-coordinated cations while the diffraction signals belonging to the (311) plane are attributed to octahedrally-coordinated cations [29–32]. Therefore the ratio between the intensity of these two signals could be taken as a useful indication for comparing the relative distribution of Ni^{2+} and Al^{3+} cations on these two sites as a function of the Ni loading of the oxide. The value of this ratio for the Ni/Al(0.50) sample was taken as a reference. The trend depicted in Fig. 2 pointed out a preferential occupancy of cations for octahedral sites for the Ni/Al(0.20), Ni/Al(0.25) and Ni/Al(0.30) samples. For lower (x < 0.20) and higher (x > 0.30) Ni/Al molar ratios, this favoured balance was less evident, thereby revealing a more comparable distribution of cations between both coordination sites.

The structural characteristics of the Ni/Al(x) catalytic precursors were further analysed by Raman spectroscopy. Fig. 3 shows the Raman spectra of the spinels with varying Ni content. The following bands at 319, 367, 593, 686 and 766 cm^{-1} could be detected for the stoichiometric Ni/Al(0.50) sample. Thus the intense band at 367 cm^{-1} and its low-frequency shoulder were assigned to the E_g and low-frequency T_{2g} modes, respectively. On the other hand, the bands at the intermediate/high-frequency region would be another T_{2g} mode (593 cm^{-1}) and various forms of the A_{1g} mode (686 and 766 cm^{-1}) [33]. This spectrum is typical of polycrystalline $NiAl_2O_4$ with an almost fully inverted cation distribution, characterised by a random occupancy of the octahedral sites by Al^{3+} and Ni^{2+} ions and a preferential occupancy of tetrahedral sites by Al^{3+} ions.

As stated previously, due to the smaller radius of Al^{3+} compared to Ni^{2+}, Ni deficiency resulted in a smaller lattice parameter of the spinel. This, along with the presence of some cation vacancies, in turn led to higher vibrational frequencies in the Raman spectra of the samples with a progressively reduced Ni/Al molar ratio. For example, the frequency of the E_g band gradually shifted from 367 cm^{-1} for the stoichiometric Ni/Al(0.50) spinel to 400 cm^{-1} for the sample with the lowest Ni loading (Ni/Al(0.13)). On the other hand, in line with XRD analysis the absence of crystalline NiO was also corroborated in view of the fact that its characteristic Raman band at 500 cm^{-1} was not noticed [34].

The surface area, pore volume and mean pore size were determined by N_2 physisorption (Table 2). According to the IUPAC classification all isotherms were type IV, indicating a mesoporous solid. The isotherms showed an H1 hysteresis, denoting a narrow distribution of uniform cylindrical pores [35]. The surface area of the stoichiometric Ni/Al(0.50) sample was 87 $m^2\ g^{-1}$. However, a significant increase was noticed for the non-stoichiometric samples, with values in the 103–119 $m^2\ g^{-1}$ range. It must be highlighted that these measured surface areas were between those of the end members of the series, 87 and 127 $m^2\ g^{-1}$ (as-synthesised γ-alumina). This enhancement of surface area was accompanied by a progressively decreasing mean pore size, from 102 Å for the stoichiometric sample to 80–91 Å for the Ni-deficient samples. However, no marked differences in the pore volume, around 0.29–0.32 $cm^3\ g^{-1}$ in all cases, were observed.

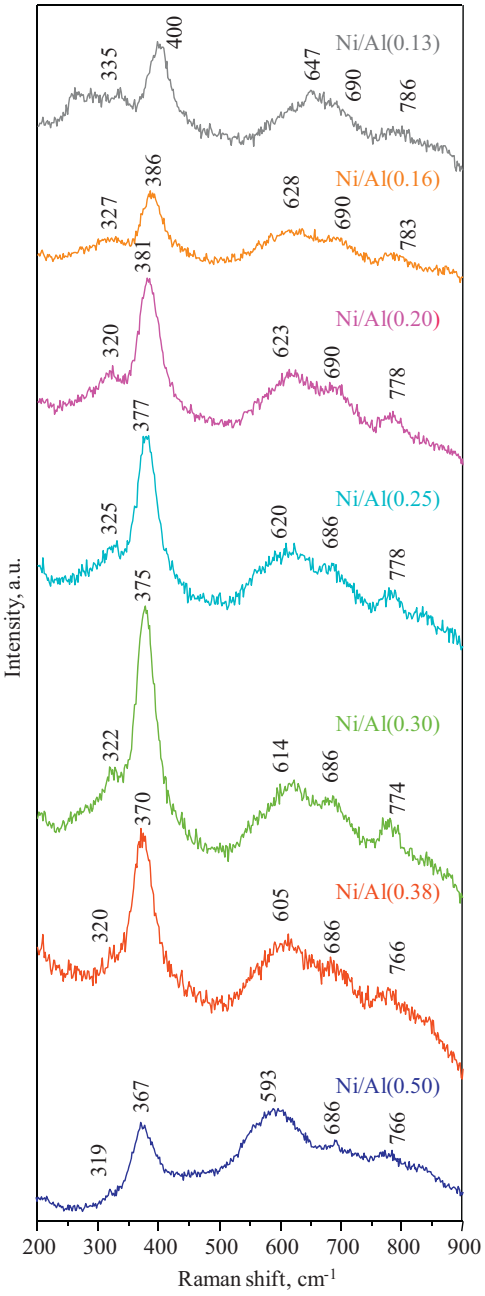

Fig. 3. Raman spectra of the Ni/Al(x) spinel-based precursors.

X-ray photoelectron spectroscopy was used to provide information about the oxidation state and the chemical environment of the nickel present on the surface of the freshly calcined spinel-type oxides. The Ni $2p_{3/2}$ spectrum of the stoichiometric Ni/Al(0.50) sample (Fig. 4) was composed of two contributions, namely the main peak corresponding to the Ni^{2+} ions and its satellite. The apparent symmetry of the Ni signal suggested the presence of a single homogeneous phase. In fact, the binding energy of this band was centred at about 855.4 eV, which was close to the theoretical value

Table 2
Composition lattice parameter and textural properties of the Ni/Al(x) spinel-based precursors.

Sample	Ni, wt.%	a_0[a], Å	Ni/Al		Calcined samples			Reduced samples		
			WDXRF	XPS	S_{BET}, $m^2\,g^{-1}$	V_p, $cm^3\,g^{-1}$	d_p, Å	S_{BET}, $m^2\,g^{-1}$	V_p, $cm^3\,g^{-1}$	d_p, Å
Ni/Al(0.50)	30.9	$8.050 \pm 1.599 \cdot 10^{-2}$	0.50	0.30	87	0.30	102	78	0.30	118
Ni/Al(0.38)	25.6	$8.038 \pm 1.245 \cdot 10^{-2}$	0.38	0.20	108	0.32	90	96	0.33	101
Ni/Al(0.30)	22.3	$8.020 \pm 9.996 \cdot 10^{-3}$	0.30	0.13	105	0.32	91	92	0.32	101
Ni/Al(0.25)	19.3	$8.007 \pm 1.103 \cdot 10^{-2}$	0.25	0.12	116	0.31	83	102	0.32	91
Ni/Al(0.20)	16.6	$7.991 \pm 9.674 \cdot 10^{-3}$	0.20	0.09	111	0.31	83	102	0.31	90
Ni/Al(0.16)	13.8	$7.975 \pm 1.651 \cdot 10^{-2}$	0.16	0.08	119	0.32	80	108	0.31	85
Ni/Al(0.13)	11.1	$7.956 \pm 1.580 \cdot 10^{-2}$	0.13	0.06	103	0.29	86	100	0.31	92

[a] The lattice parameter and the surface area of the as-synthesised γ-Al_2O_3 were 7.891 Å and 127 $m^2\,g^{-1}$, respectively.

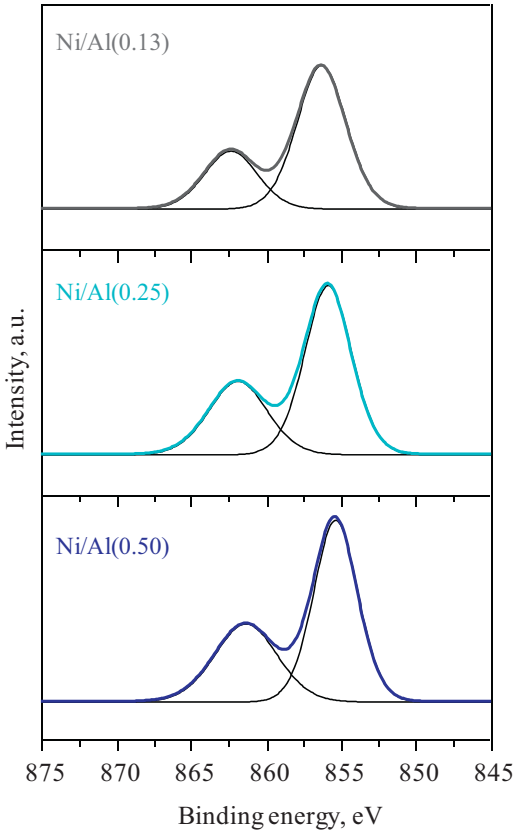

Fig. 4. XPS spectra of Ni $2p_{3/2}$ region of the Ni/Al(x) spinel-based precursors: (a) Ni/Al(0.50), (b) Ni/Al(0.25) and (c) Ni/Al(0.13).

for the nickel aluminate phase (856.0 eV). Moreover, the separation between the principal peak and its satellite (6.0 eV) matched with the reference value (6.3 eV) corresponding to the nickel aluminate spinel [36]. In relation to the XPS spectra of the substoichiometric samples and, in agreement with the results from Ubaid and Wolf [15], no significant changes in the binding energies of the Ni $2p_{3/2}$ line were found with respect to the stoichiometric spinel. As an example, the spectra of the Ni/Al(0.25) and Ni/Al(0.13) oxides are plotted in Fig. 4. Thus it was corroborated that irrespective of the Ni/Al molar ratio the surface nickel was primarily in the form of the aluminate structure. In addition to the nature and oxidation state of nickel, XPS also offered valuable information regarding the surface composition. The values of the bulk and surface Ni/Al ratios as determined by WDXRF and XPS, respectively, are listed in Table 2. In all samples the Ni/Al ratio (analysed up to a depth of about 5 nm) was about two times (1.7–2.3) lower than the ratio given by WDXRF (Table 2), which may indicate that a nickel-deficient aluminium-rich phase existed on the surface of the spinels.

The coordination and the oxidation state of nickel species on the surface of the various spinel-type oxides were studied by means of diffuse reflectance spectroscopy. The corresponding DRS spectra of the seven prepared samples, along with that of the as-synthesised γ-Al_2O_3, are shown in Fig. 5. It was noticed that these patterns resulted almost identical regardless of the Ni/Al molar ratio. Hence, all spectra displayed a strong absorption in the UV domain. The maxima centred at 220–345 nm (not shown) were ascribed to $O^{2-} \rightarrow Ni^{2+}$ metal to ligand charge transfers [37]. In the visible range the bands located at 380 and 720 nm were associated with ν_3 ($^3A_{2g} \rightarrow {}^3T_{1g}$ (P)) and ν_2 ($^3A_{2g} \rightarrow {}^3T_{1g}$) absorptions that resulted from d-d transitions of Ni^{2+} ions hosted by octahedral sites [23]. The relative low intensity of these bands implied that the detected Ni^{2+} in an octahedral environment was not ascribable to the presence of massively segregated NiO phase but to Ni^{2+} ions belonging to the nickel aluminate lattice [18]. The spectra were also characterised by the presence of an additional intense band at 600–645 nm and shoulders at 550 nm and 760 nm, assigned to the ($^3T_1$(F) → $^3T_{1g}$ (P)) ligand transitions, thereby evidencing the presence of the tetrahedrally coordinated Ni^{2+} ions [36]. In sum, DRS spectra confirmed the existence of nickel ions in tetrahedral and in octahedral sites consistently with the formation of a spinel structure. Therefore, the nickel aluminate phase observed in all samples could be described as a partial inverse spinel since Ni^{2+} ions occupied both octahedral and tetrahedral positions of the lattice.

In the NIR domain a broad band located around 1120 nm was noticed which was attributed to the ν_1 ($^3A_{2g} \rightarrow {}^3T_{2g}$) transition of Ni^{2+} in octahedral symmetry [38]. It was noticed that the position of this band steadily shifted to lower wavelengths (1020 nm for the Ni/Al(0.13) sample) when decreasing the Ni loading of the sample [39]. The area of this band could indeed provide useful information about the relative amount of Ni^{2+} ions hosted by octahedral sites in the spinelic lattice of the various samples. Thus, taking the area under this band for the Ni/Al(0.50) sample as a reference, the relative population of this kind of species present in each sample could be compared. Results included in Fig. 5 indicated that the occupancy of Ni^{2+} ions on octahedral sites was favoured for samples with an intermediate (x = 0.20–0.38) Ni/Al molar ratio, namely the Ni/Al(0.20), Ni/Al(0.25), Ni/Al(0.30) and Ni/Al(0.38) samples. This trend was consistent with the results from XRD which indicated a favoured octahedral coordination of cations for these samples. In short, these data suggested that Ni^{2+} ions tended to migrate from the tetrahedral sites to the octahedral sites when the Ni present in the oxide decreased from 31 to 17 wt.%. It is thought that Ni^{2+} cations, because of their high crystal field stabilisation energy in octahedral symmetry, were prone to preserve this coordination. Analogously, Rotan et al. [40] also noticed that the location of Ni^{2+} on octahedral sites was favoured with respect to the tetrahedral ones as the Ni content was lower for a set of NiO-Al_2O_3 solid solutions with a Ni/Al molar ratio between 0.44 and 0.50. For lower Ni contents (x < 0.16) the migration was reverted and the occupancy of tetrahedral sites was again promoted.

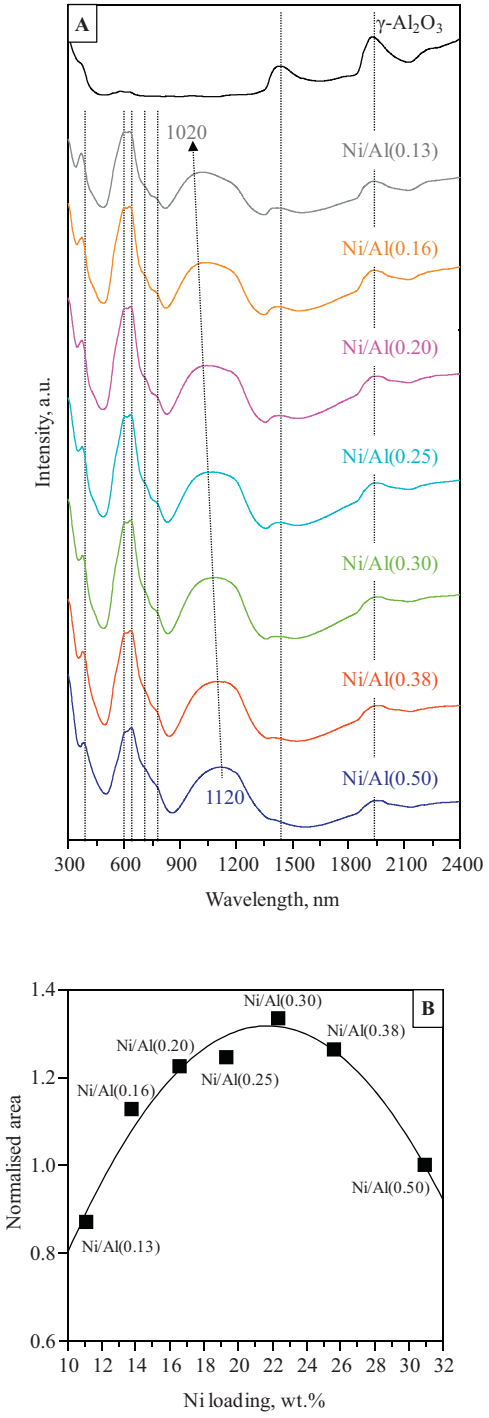

Fig. 5. UV–vis-NIR DRS spectra of the Ni/Al(x) spinel-based precursors (A). Evolution of the normalised area of the band in the 850–1400 nm range as a function of the composition of the spinel (B).

Besides, the presence of traces of segregated alumina in all Ni/Al(x) samples was revealed as the characteristic bands of this phase at higher wavelengths (1530 cm^{-1} and 1930 cm^{-1}) were detected. Moreover, it was observed that as the nickel content decreased, and consequently the fraction of alumina increased, the intensity of these features progressively became more pronounced. This finding could be considered as an additional evidence for the enrichment of the surface of the spinels with aluminium-rich species as revealed by XPS.

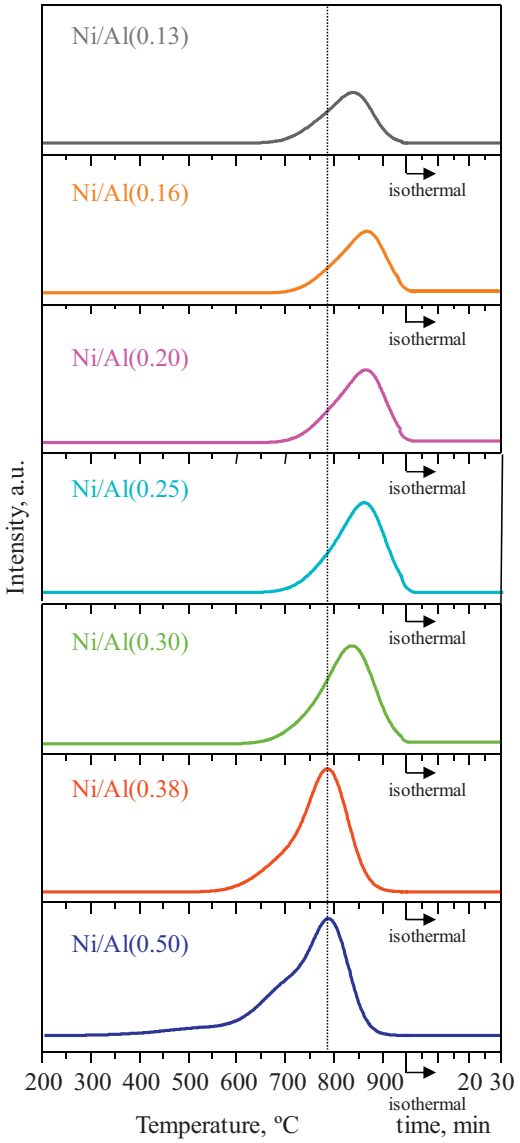

Fig. 6. H_2-TPR profiles of the calcined Ni/Al(x) spinel-based precursors.

Finally, the reducibility of the samples was examined by temperature-programmed reduction with H_2 up to 950 °C with a subsequent isothermal step for 0.5 h. Fig. 6 compares the reduction profiles of the various spinels while Table 3 lists the experimental and theoretical H_2 uptakes. In this sense it should be pointed out that a good agreement was found between both values for each sample, thereby confirming that the reduction of Ni^{2+} cations was always complete. The stoichiometric sample exhibited a broad reduction profile with a distinct reduction peak at about 790 °C, typically associated with the reduction of the nickel aluminate phase [20]. The shoulder at about 650 °C was related to the reduction of the surface of the spinel. Also a small contribution was observed at around 450 °C related to the reduction of free NiO species not properly incorporated in the spinel lattice [41]. The contribution of the H_2 uptake of this species accounted for 10% of the overall consumption. It was noteworthy that this phase (NiO) was not visible in the XRD pattern, probably due to the fact that its crystallite size was very small and/or it was highly dispersed on the surface of the spinel. As for the non-stoichiometric samples the onset for H_2 consumption shifted towards higher temperatures, in the 500–625 °C range, in comparison with 350 °C for the Ni/Al(0.50) sample. As a consequence, the reduction process occurred at a progressively

Table 3
Reducibility of the Ni/Al(x) spinel-based precursors and metallic particle size, dispersion and surface area of the reduced Ni/Al(x) catalysts.

Sample	H_2 uptake[a], mmol g^{-1}	Degree ofreduction (850 °C), %	Peak reductiontemperature, °C	d_{Ni}, nm		D, %	S_{Ni}, m^2 g^{-1}
				XRD	TEM		
Ni/Al(0.50)	5.3 (5.5)	98	785	9	12	10	17
Ni/Al(0.38)	4.4 (4.5)	84	785	11	13	9	13
Ni/Al(0.30)	3.8 (3.8)	66	840	14	16	8	9
Ni/Al(0.25)	3.3 (3.3)	48	860	15	21	6	6
Ni/Al(0.20)	2.8 (2.5)	52	870	13	13	9	8
Ni/Al(0.16)	2.3 (2.1)	47	870	13	12	10	7
Ni/Al(0.13)	1.9 (1.8)	71	840	15	21	6	3

[a] Values in parentheses corresponded to experimental data.

narrower temperature window as the Ni/Al molar ratio was lower. A similar narrowing of the reduction temperature window was also found by Shang et al. [42] for Ni-Al composite oxides with a Ni/Al molar ratio in the 0.25–0.10 range. These two findings along with the absence of a distinct shoulder at low temperatures in the main reduction peak suggested that the reduction of both surface and bulk of the Ni-deficient spinels occurred simultaneously.

Likewise the reduction peak gradually shifted to higher temperatures from 790 to 870 °C for decreasing Ni/Al molar ratios from 0.50 to 0.16. Only the Ni/Al(0.13) spinel with the lowest Ni content exhibited a somewhat lower reduction peak at about 840 °C. This overall behaviour pointed out that an excess of alumina clearly stabilised the resultant spinel phase. Similarly, Salhi et al. [16] also noticed an inhibition of reducibility for spinels with increasing Ni deficiency. Furthermore, the relationship between the reducibility and the composition of the spinel could be better understood by analysing the degree of reduction at a given temperature (850 °C). It was noticed that the reducibility steadily diminished as the Ni loading decreased (Table 3), being the lowest, around 47–52%, for the Ni/Al(0.25), Ni/Al(0.20) and Ni/Al(0.16) samples. In view of the results from XRD and UV–vis-NIR DRS it could be then stated that the favoured presence of Ni cations with an octahedral coordination resulted in an inhibited reducibility.

On the other hand, with the aim of verifying that the proposed reduction step (at 850 °C for 2 h) used prior to catalytic runs was adequate to achieve a complete reduction of nickel species, the H_2-TPR run was conducted according to this activation protocol. Judging from its higher stability the Ni/Al(0.25) sample was analysed as a reference. It was found that under these conditions a full reduction of this nickel precursor was again attained. It could be therefore assumed that all spinel catalysts would achieve a 100% degree of conversion from Ni^{2+} to metallic nickel (Ni^0) under the conditions selected for in situ reduction in the reactor. Obviously these conditions ensured the reduction of the eventual presence of free NiO in the spinelic precursors.

3.3. Characterisation of the reduced catalysts

Next the results on the characterisation of the various Ni-based spinel precursors submitted to the activation step by high-temperature reduction will be discussed. Thus, the Ni/Al_2O_3 catalysts were analysed by N_2 physisorption, XRD and TEM. As far as the textural properties were concerned the surface area of the freshly reduced spinel catalysts somewhat decreased with respect to its corresponding calcined counterpart. However, when compared with the reduced stoichiometric sample, again higher values were evidenced for samples with Ni deficiency. The pore size was slightly larger (85–101 Å) with respect to the calcined counterparts (80–91 Å). Apparently the pore volume was not affected by high-temperature reduction since it was very similar for all samples (0.30–0.32 cm^3 g^{-1}), and also close to the values of the calcined spinels.

The mean Ni particle size was estimated by XRD from the Ni (200) signal at $2\theta = 51.7°$ (Fig. S3). Results listed in Table 3 suggested that the substoichiometric samples were characterised by a slightly larger crystallite size (11–15 nm) with respect to the Ni/Al(0.50) sample (9 nm). Note that the presence of NiO in the stoichiometric sample did not induce the formation of large particles after reduction [21]. A closer inspection of the relationship of this feature with the composition indicated that the size increased up to attain a maximum value (15 nm for the Ni/Al(0.25) sample) and then decreased for the catalysts with a lower Ni loading. Only the Ni/Al(0.13) sample with a size of 15 nm deviated from this general relationship. As will be shown later on, this divergence could be related to a noticeably larger heterogeneity of the particle size distribution. Recall that in all cases the diffraction patterns only revealed the characteristic signals of metallic nickel and alumina.

The reduced samples were further characterised by TEM from the measurement of the size of more than 175 particles. The corresponding histograms and profiles of accumulated frequency are depicted in Fig. S4 while the surface mean particle sizes are summarised in Table 3. The sizes were in the 12–21 nm range, being the largest values for the Ni/Al(0.25) and Ni/Al(0.13) samples, consistently with the XRD results. Particularly significant was the presence of a large amount (35%) of particles with a considerably large size (20 nm), which was responsible for the larger surface mean size measured for this latter catalyst. When compared with XRD data it was reasonable to assume that active nickel particles were small aggregates of crystallites, thereby proving the polycrystalline nature of the samples. Thus, on average it seemed that each particle consisted of about two Ni crystallites. On the other hand, from the nickel particle size measured by TEM the dispersion and accessible metallic surface were calculated according to the methodology proposed by Borodziński and Bonarowska [43]. These values (Table 3) evidenced that the reduced stoichiometric spinel definitely exhibited the largest metallic surface area (17 m^2_{Ni} g^{-1}) followed by the Ni/Al(0.38) sample with 13 m^2_{Ni} g^{-1}. The catalysts with a Ni/Al molar ratio between 0.16 and 0.30 exhibited a similar metallic area (6–9 m^2_{Ni} g^{-1}) while for the spinel with the largest Ni deficiency this was even lower (3 m^2_{Ni} g^{-1}). Note that the lower value of the Ni/Al(0.13) with a nickel loading of 11 wt.% was expected due to its considerably large crystallite size (21 nm). In line with the analysis by XRD and UV–vis-NIR DRS it was clearly found that both nickel particle size and available metallic surface area greatly depended on the relative occupancy of nickel ions on octahedral and tetrahedral sites in the spinelic lattice, which in turn was a function of the Ni loading of the spinel. Thus a relatively higher abundance of nickel cations with an octahedral coordination led to samples with larger particles and lower metallic areas in comparison with the stoichiometric sample.

As stated earlier a volcano-type relationship between the yield of hydrogen and the composition of the Ni-deficient Ni/Al(x) spinel catalyst was found for the partial oxidation of methane at low temperatures. In this way, in relation with the Ni/Al(0.50) cat-

alyst a similar performance was noticed for the sample with a Ni loading of 19 wt.%, which was markedly lower than the metal content of the stoichiometric nickel aluminate (31 wt.%). From a practical point of view this meant an interesting advantage provided by this kind of substoichiometric spinel oxides. While being the investigated reduced Ni/Al(x) catalysts stable with time on stream, the activity trend was however verified not to be affected by eventual changes in their physico-chemical properties. Hence the characterisation of the post-run samples evidenced no coke formation as revealed by TGA-MS and a considerable thermal and chemical stability of the nickel particles since neither sintering nor oxidation was detected by XRD. As for sintering it is interesting to note that although the inlet temperature increased up to 725 °C at the beginning of the reaction, this was well below 850 °C, which was the temperature of the activation step.

The analysis of both characterisation and kinetic data of the freshly reduced catalysts revealed that the oxidation behaviour was not linearly dependent on the available metallic surface area since the yield of hydrogen was maximised over the Ni/Al(0.25) and Ni/Al(0.50) catalysts with a substantially different values of this property (6 and 17 $m^2_{Ni}\,g^{-1}$, respectively). The notable performance of the Ni/Al(0.25) catalyst with this low surface area was even more striking since this sample, on account of its metal content and BET surface area, was the one that theoretically is closer to the formation of a Ni monolayer (34.4 $\mu mol_{Ni}\,m^{-2}$) and therefore closer to the optimal nickel dispersion. Surprisingly this spinel was characterised by a considerably low metallic surface area as determined by TEM in comparison with the Ni/Al(0.50) sample. This finding clearly suggested that other more complex factors were responsible for the observed relationship between the properties of the metallic sites and activity. Thus, these features appeared to be connected with the structural changes provoked by Ni deficiency in the lattice of the spinel. Particularly excess of alumina induced a variation of the coordination environment of Ni^{2+} ions.

It was proposed that the good behaviour of the stoichiometric sample could be attributed to its remarkably high metallic surface area, which was mainly generated from Ni^{2+} located at tetrahedral sites. Nevertheless, when the Ni/Al ratio decreased the relative population of nickel cations on octahedral sites increased. In spite of the fact that the reduction of these kind of cations required high temperatures and led to lower metallic surface areas, this did not appear to dramatically affect the catalytic behaviour as the Ni/Al(0.30), Ni/Al(0.20) and particularly Ni/Al(0.25) gave remarkable kinetic results with 6–9 $m^2_{Ni}\,g^{-1}$. Note that the degree of occupancy for octahedral sites was properly balanced for these three spinel precursors. In sum, although after high-temperature reduction catalysts with a lower metallic dispersion (6–8%) were obtained, it could be concluded that stronger metal-supports were created, thereby resulting in a superior specific activity of the Ni particles present in these samples, which was derived from Ni^{2+} cations with a preferential octahedral coordination. All these structural changes were responsible for the comparable performance of the Ni/Al(0.25) catalyst with respect to the stoichiometric sample. On the other hand, the poor catalytic behaviour of the Ni/Al(0.38) catalyst with a Ni loading of 26 wt.% deserves a proper explanation since it also exhibited a high relative population of nickel cations with an octahedral coordination. However, due to its noticeably high metal loading, it should be expected that a large fraction of nickel cations still occupied tetrahedral sites. Since the activity of metallic nickel derived from cations with this coordination was lower than that of octahedral cations, both conversion and yield of hydrogen of this sample were not as high as those found over the Ni/Al(0.50) and Ni/Al(0.30) catalysts.

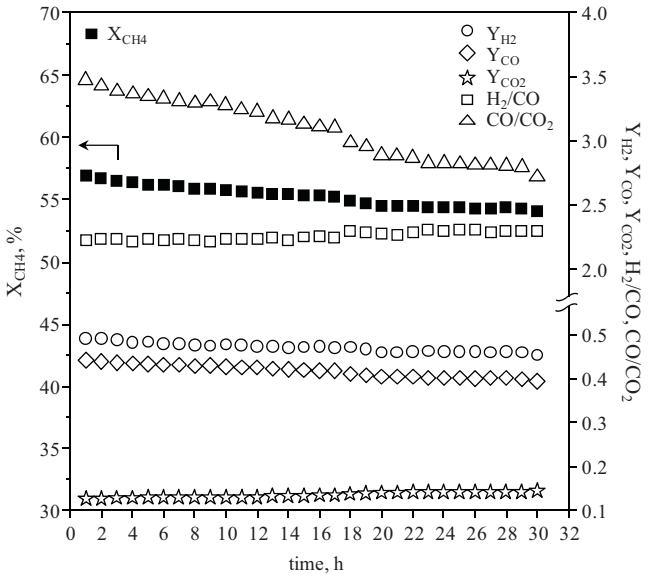

Fig. 7. Evolution of methane conversion and product distribution as a function of time on stream over the Ni/Al(0.25) catalyst (reaction conditions: O/C = 0.8; 60000 mL $CH_4\,g^{-1}\,h^{-1}$; 650 °C; 30 h).

3.4. Catalytic behaviour of the Ni/Al(0.25) catalyst under severe reaction conditions

Since the Ni/Al(0.25) sample gave an activity comparable to that shown by the stoichiometric sample with a considerably lower Ni loading (19 wt.%), it would be necessary to assess its promising potential by evaluating its performance under more severe reaction conditions. For this purpose the VHSV was increased up to 60000 mL $CH_4\,g^{-1}\,h^{-1}$, a substoichiometric oxygen feed (O/C = 0.8) was employed and the reaction time was extended up to 30 h. The evolution of methane conversion and yield of hydrogen as a function of time on stream is plotted in Fig. 7. Initially the catalyst achieved a 57% conversion. However, the activity slowly decreased with time on line to give a 54% conversion at the end of the run. Correspondingly, the yield of hydrogen progressively shifted from 0.49 to 0.45. The equilibrium value was 0.83. In view of these results the catalytic behaviour could be considered relatively stable as a decrease in conversion and yield of hydrogen by 5 and 8% was found, respectively. Finally, the average H_2/CO and CO/CO_2 ratios were 2.3 and 3.1, respectively.

In order to gain insight into the noticeable performance of this catalyst, the spent sample was thoroughly characterised by XRD, BET measurements, TGA-MS, TEM and Raman spectroscopy. XRD analysis was helpful in characterising the state of the metallic phase and revealing the eventual presence of graphitic carbon. The diffraction pattern (Fig. S5) of the post-run sample evidenced, on one hand, the absence of NiO phase and, on the other hand, the absence of sintering since the crystallite size remained unaltered after reaction (15 nm). As for coking the presence of graphitic carbon was confirmed as the signal at $2\theta = 26.6°$ (JCPDS 89-8487) was clearly visible. Nevertheless, owing to the fact that the eventual formation of amorphous carbon could not be detected by XRD, the post-reaction sample was additionally characterised by Raman spectroscopy (Fig. S6). After curve fitting of the spectrum using Lorentzian lines two main bands at 1360 and 1580 cm^{-1} along with a shoulder band at 1610 cm^{-1} were distinguished. The signals at 1360 (the so-called D band) and 1610 cm^{-1} (denoted as D' band) are associated with carbon with structural imperfections while the band at 1580 cm^{-1} (the so-called G band) is related to graphite layers. Taking the ratio of the areas of D and G bands (I_D/I_G) as an index

for the crystalline order of deposited filaments, it was found that both amorphous and graphitic filamentous carbon were formed on the catalyst, with a similar distribution ($I_D/I_G = 1.1$).

On the other hand, the specific surface area of the post-run sample considerably decreased from 102 $m^2\,g^{-1}$ for the freshly reduced sample to 74 $m^2\,g^{-1}$, owing to the blockage of the pores caused by coking. The total amount of coke deposited on the spent catalyst and its combustion temperature were determined by TGA-MS. Fig. S7 shows the derivative thermogravimetric change versus temperature. The combustion of coke occurred in the 400–700 °C temperature range, with an oxidation peak centred at 575 °C accompanied by a shoulder at lower temperatures (450 °C). According to the temperature range required for the complete combustion it could be stated that formed coke was filamentous carbon, which was around 14%. When referred to the achieved conversion and the reaction time interval the average coke formation rate was 10.5 μmol C $mol_{converted\ CH4}^{-1}\,h^{-1}$. TEM images (Fig. S8) further confirmed that the used catalyst was mainly covered with deposits with this morphology. The observed coke formation was in agreement with the nickel particle size of the sample (15 nm) since it is known that this deposition is favoured for particles above a certain critical size, around 5 nm [44,45]. In sum, coking was responsible for the slight loss of both conversion and yield of hydrogen with time on line. While the impact of coking on the H_2/CO was hardly visible a more marked effect on the CO/CO_2 molar ratio was noted as a consequence of the increased yield of CO_2 and decreased yield of CO with time on stream (Fig. 7). Thus the CO/CO_2 ratio steadily diminished from 3.5 to 2.7. These observations were coherent with the formation of coke as a consequence of the CO disproportionation reaction ($2CO \rightarrow C + CO_2$).

4. Conclusions

The catalytic activity of a number of nickel aluminate-based precursors with varying Ni/Al ratios was examined for the partial oxidation of methane at relatively low temperatures. Interestingly the composition of the Ni-deficient spinels could be optimised in such a way that a comparable performance could be obtained with respect to the stoichiometric sample (31 wt.%Ni). This suitable Ni/Al ratio of the substoichiometric precursor was 0.25, which corresponded to a 19 wt.%Ni loading.

Samples with a deficiency of nickel preserved a spinel-type structure with no apparent segregation of NiO although a small fraction of γ-alumina could be detected on the surface of the samples. On the other hand, the increased alumina excess in the lattice induced a marked stability of the resultant aluminate phase as revealed by the higher temperatures required for full reduction. This inhibition of the transformation of Ni^{2+} cations into metallic nickel was correlated with the observed preferential occupancy of these ions for octahedral sites in the spinelic lattice. This favoured distribution on octahedral sites could be optimised by tuning the Ni/Al molar ratio at values around 0.25–0.30. After activation at high-temperature reduction of these substoichiometric precursors a significant sintering was certainly observed, which in turn led to lower available metallic surface areas.

The activity trend found for the investigated alumina supported nickel catalysts derived from substoichiometric spinel-based precursors indicated that the remarkable performance of the Ni/Al(0.25) sample could be related to a higher specific activity of crystallites derived from Ni^{2+} cations located at octahedral sites in spite of the fact that the reduction of these metallic species resulted in larger crystallite sizes and lower metallic surface areas (6 $m^2_{Ni}\,g^{-1}$). This was in contrast with the lower intrinsic oxidation power of crystallites preferentially generated from Ni^{2+} on tetrahedral sites in the stoichiometric sample (17 $m^2_{Ni}\,g^{-1}$). Apparently these two effects (metallic specific activity and surface area) were mutually compensated, thereby leading to a comparable catalytic behaviour.

A further analysis of this promising Ni/Al(0.25) catalyst under more severe reaction conditions evidenced both notable activity and stability with time on stream. After reaction no sintering was evident. Moreover, the significant formation of carbonaceous graphitic filaments did not seem to play a marked negative effect on activity, probably owing to the fact that accessibility to active metallic sites was still preserved.

Acknowledgements

The authors wish to thank the financial support for this work provided by the Spanish Ministry of Economy and Competitiveness (ENE2013-41187-R) and the Basque Country Government (PRE_2015_2_0114). Technical and human support from SGIker (WDXRF (F.J. Sangüesa), XRD (A. Larrañaga), XPS (B. Sánchez), Raman spectroscopy (A. Sarmiento), UV–vis-NIR DRS (L. Bartolomé) and TEM (A. Martínez)) is also gratefully acknowledged.

Appendix A. Supplementary data

Supplementary data associated with this article can be found, in the online version, at http://dx.doi.org/10.1016/j.apcatb.2017.02.063.

References

[1] W. Chu, W. Yang, L. Lin, Appl. Catal. A: Gen. 235 (2002) 39–45.
[2] T.H. Gardner, J.J. Spivey, A. Campos, J.C. Hissam, E.L. Kugler, A.D. Royd, Catal. Today 157 (2010) 166–169.
[3] Z. Jiang, J. Su, M.O. Jones, H. Shi, T. Xiao, P.P. Edwards, Energy Fuels 23 (2009) 1634–1639.
[4] J. Zhang, N. Zhao, W. Wei, Y. Sun, Int. J. Hydrogen Energy 35 (2010) 11776–11786.
[5] L.D. Vella, J.A. Villoria, S. Specchia, N. Mota, J.L.G. Fierro, V. Specchia, Catal. Today 171 (2011) 84–96.
[6] T.H. Nguyen, A. Łamacz, P. Beaunier, S. Czajkowska, M. Domański, A. Krztoń, T.V. Le, G. Djéga-Mariadassou, Appl. Catal. B: Environ. 152–153 (2014) 360–369.
[7] M. Sturzenegger, L. D'souza, R.P.W.J. Struis, S. Stucki, Fuel 85 (2006) 1599–1602.
[8] F.F. Tao, J. Shan, L. Nguyen, Z. Wang, S. Zhang, L. Zhang, Z. Wu, W. Huang, S. Zeng, P. Hu, Nat. Commun. 6 (2015) 1–10, http://dx.doi.org/10.1038/ncomms8798.
[9] J.N. Roelofsen, R.C. Peterson, Am. Miner. 77 (1992) 522–528.
[10] B. Roy, K. Loganathan, H.N. Pham, A.K. Datye, C.A. Leclerc, Int. J. Hydrogen Energy 35 (2010) 11700–11708.
[11] N. Salhi, A. Boulahouache, C. Petit, A. Kiennemann, C. Rabia, Int. J. Hydrogen Energy 36 (2011) 11433–11439.
[12] C. Jiménez-González, Z. Boukha, B. de Rivas, J.R. González-Velasco, J.I. Gutiérrez-Ortiz, R. López-Fonseca, Energy Fuels 28 (2014) 7109–7121.
[13] C. Sprung, B. Arstad, U. Olsbye, ChemCatChem 6 (2014) 1969–1982.
[14] D.F.P. Suffredini, V.V. Thyssen, P.M.M. de Almeida, R.S. Gomes, M.C. Borges, A.M. Duarte de Farias, E.M. Assaf, M.A. Fraga, S.T. Brandão, Catal. Today (2016), http://dx.doi.org/10.1016/j.cattod.2016.07.027.
[15] A.A. Ubaid, E.E. Wolf, Appl. Catal. A: Gen. 40 (1998) 73–85.
[16] N. Salhi, C. Petit, A.C. Roger, A. Kiennemann, S. Libs, M.M. Bettahar, Catal. Today 113 (2006) 187–193.
[17] L. Zhang, X. Wang, X. Shang, M. Tan, W. Ding, X. Lu, J. Energy Chem. 26 (2016) 93–100.
[18] G. Wu, C. Zhang, S. Li, Z. Han, T. Wang, X. Ma, ACS Sustain. Chem. Eng. 1 (2013) 1052–1062.
[19] Z. Boukha, C. Jiménez-González, B. de Rivas, J.R. González-Velasco, J.I. Gutiérrez-Ortiz, R. López-Fonseca, Appl. Catal. B: Environ. 158–159 (2014) 190–201.
[20] C. Jiménez-González, M. Gil-Calvo, B. de Rivas, J.R. González-Velasco, J.I. Gutiérrez-Ortiz, R. López-Fonseca, Ind. Eng. Chem. Res. 55 (2016) 3920–3929.
[21] Z. Boukha, C. Jiménez-González, M. Gil-Calvo, B. de Rivas, J.R. González-Velasco, J.I. Gutiérrez-Ortiz, R. López-Fonseca, Appl. Catal. B: Environ. 199 (2016) 372–383.
[22] R. López-Fonseca, C. Jiménez-González, B. de Rivas, J.I. Gutiérrez-Ortiz, Appl. Catal. A: Gen. 437–438 (2012) 53–62.
[23] B.C. Enger, R. Lødeng, J. Walmsley, A. Holmen, Appl. Catal. A: Gen. 383 (2010) 119–127.
[24] P. Kim, Y. Kim, H. Kim, I.K. Song, J. Yi, Appl. Catal. A: Gen. 272 (2004) 157–166.

[25] C. Otero Arean, M. Penarroya Mentruit, A.J. López López, J.B. Parra Soto, Colloid Surf. A: Physicochem. Eng. Aspect 180 (2001) 253–258.
[26] J.S. Yoo, A.A. Bhattacharyya, C.A. Radlowski, Ind. Eng. Chem. Res. 30 (1991) 1444–1448.
[27] H. Cui, M. Zayat, D. Levy, J. Non Cryst. Solids 351 (2005) 2102–2106.
[28] M. Hasan, J. Drazin, S. Dey, R.H.R. Castro, Am. Miner. 100 (2015) 652–657.
[29] N.F.P. Ribeiro, R.C.R. Neto, S.F. Moya, M.M.V.M. Souza, M. Schmal, Int. J. Hydrogen Energy 35 (2010) 11725–11732.
[30] Y.S. Han, J.B. Li, X.S. Ning, B. Chi, J. Am. Ceram. Soc. 87 (2004) 1347–1349.
[31] A. Tirsoaga, D. Visinescu, B. Jurca, A. Ianculescu, O. Carp, J. Nanopart, J. Nanopart. Res. 13 (2011) 6397–6408.
[32] C. Ragupathi, J.J. Vijaya, P. Surendhar, L.J. Kennedy, Polyhedron 72 (2014) 1–7.
[33] M.A. Laguna-Bercero, M.I. Sanjuán, R.I. Merino, J. Phys. Condens. Matter 19 (2007) 186217–186227.
[34] A.V. Ghule, K. Ghule, S.H. Tzing, T.H. Punde, H. Chang, Y.C. Ling, J. Solid State Chem. 182 (2009) 3406–3411.
[35] M. Thommes, K. Kaneko, A.V. Neimark, J.P. Olivier, F. Rodriguez-Reinoso, J. Rouquerol, K.S.W. Sing, Pure Appl. Chem. 87 (2015) 1051–1069.
[36] J.L. Rogers, M.C. Mangarella, A.D. D'Amico, J.R. Gallagher, M.R. Dutzer, E. Stavitski, J.T. Miller, C. Sievers, ACS Catal. 6 (2016) 5873–5886.
[37] C. Jiménez-González, Z. Boukha, B. de Rivas, J.J. Delgado, M.A. Cauqui, J.R. González-Velasco, J.I. Gutiérrez-Ortiz, R. López-Fonseca, Appl. Catal. A: Gen. 466 (2013) 9–20.
[38] H. Cai, G.C. Farrington, J. Electrochem. Soc. 139 (1992) 744–748.
[39] G. Garbarino, P. Riani, A. Infantes-Molina, E. Rodríguez-Castellón, G. Busca, Appl. Catal. A: Gen. 525 (2016) 180–189.
[40] M. Rotan, J. Tolchar, E. Rytter, M.A. Einarsrud, T. Grande, J. Solid State Chem. 182 (2009) 3412–3415.
[41] F.G.E. Nogueira, P.G.M. Assaf, H.W.P. Carvalho, E.M. Assaf, Appl. Catal. B: Environ. 160–161 (2014) 188–189.
[42] X. Shang, X. Wang, X. Zou, X. Lu, W. Ding, J. Porous Mater. 22 (2015) 1153–1160.
[43] A. Borodziński, M. Bonarowska, Langmuir 13 (1997) 5613–5620.
[44] D. Chen, K.O. Christensen, E. Ochoa-Fernández, Z. Yu, B. Tøtdal, N. Latorre, A. Monzón, A. Holmen, J. Catal. 229 (2005) 82–96.
[45] H. Ozdemir, M.A. Faruk Oksuzomer, M. Ali Gurkaynak, Int. J. Hydrogen Energy 35 (2010) 12147–12160.